IS-T-809

THERMAL AND ELECTRICAL CONDUCTIVITIES OF HIGH PURITY TANTALUM

Scott Lee Archer

M.S. Thesis Submitted to Iowa State University

Ames Laboratory, USDOE
Iowa State University
Ames, Iowa 50011

Date Transmitted: January 1978

PREPARED FOR THE U.S. DEPARTMENT OF ENERGY UNDER CONTRACT NO. W-7405-eng-82

DISCLAIMER

NOTICE

Available from: National Technical Information Service
U. S. Department of Commerce
P.O. Box 1553
Springfield, VA 22161

Price: Microfiche $3.00

Thermal and Electrical Conductivities of High Purity Tantalum

by

Scott Lee Archer

A Thesis Submitted to the
Graduate Faculty in Partial Fulfillment of
The Requirements for the Degree of
MASTER OF SCIENCE

Approved:


In Charge of Major Work

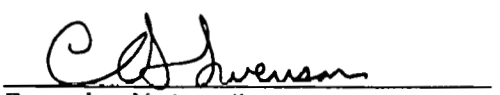
For the Major Department

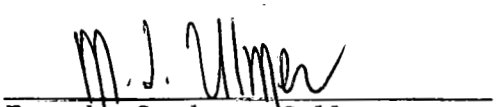
For the Graduate College

Iowa State University
Ames, Iowa

1978

TABLE OF CONTENTS

LIST OF TABLES

LIST OF FIGURES

Thermal and electrical conductivities

of high purity tantalum

Scott Lee Archer

Under the supervision of Gordon C. Danielson
From the Department of Physics
Iowa State University

The electrical resistivity and thermal conductivity of three high purity tantalum samples have been measured as functions of temperature over a temperature range of 5K to 65K. Sample purities ranged up to a resistivity ratio of 1714. The highest purity sample had a residual resistivity of $.76 \times 10^{-10}\Omega$-m. The intrinsic resistivity varied as $T^{3.9}$ from 10K to 31K. The thermal conductivity of the purest sample had a maximum of 840 W/mK at 9.8K. The intrinsic thermal resistivity varied as $T^{2.4}$ from 10K to 35K. At low temperatures electrons were scattered primarily by impurities and by phonons with both interband and intraband transitions observed. The electrical and thermal resistivity is departed from Matthiessen's rule at low temperatures.

CHAPTER I: INTRODUCTION

Literature Review

Tantalum is a group 5 b transition metal below vanadium and niobium in the periodic table. Tantalum exhibits a valence of five and, to a lesser extent, three (1). The metal has a body-centered cubic structure at 20°C with a lattice constant of 3.3026Å. It is a type II superconductor with a critical temperature of 4.483K; however the temperature varies somewhat with sample purity (2). Several different values of the Debye temperature are reported (1,2,3,4) varying from 230K to 266K. Killean and Lisher (4), using previously measured elastic constants, calculated a Debye temperature of 266K.

The first relatively pure ductile tantalum was produced in 1903 by Von Bolton (2). Tantalum is mined as the mineral columbite-tantalite $(Fe,Mn)(Nb,Ta)_2O_6$. Once the niobium and tantalum are obtained from the ore, one of several commercial methods is used to separate the tantalum from the niobium. They include: electrolysis of molten potassium fluotantalate, reduction of potassium fluotantalate with sodium, and reacting tantalum carbide with tantalum oxide (2).

Tantalum, with a melting point of 2996°C, is used in alloys with desirable properties such as high melting point, high strength and good ductility.

Early investigations of the low temperature transport properties of tantalum were hampered by the relatively impure samples available. The high concentration of impurities lead to impurity scattering, which

is dominant at low temperatures, and masks any intrinsic effects of the lattice.

Mendelssohn and Olson, in 1950 (5); Mendelssohn and Rosenberg, in 1952 (6); and White and Woods, in 1959 (3), measured the low temperature thermal conductivity of tantalum with purities up to 99.98%. This purity corresponds to a relative resistivity ratio (RRR) of 590. The RRR is the ratio of the resistivity at 295K to the resistivity at 4.2K and is a commonly employed method to determine the amount of impurities. These samples were of sufficient purity to exhibit a maximum in the thermal conductivity around 24K. The largest value obtained for this maximum was 148 W/m-K by White and Woods. The peak shifted to lower temperatures as purity increased but never lower than 21K. Powell and Blanpied (7) reported that between 8K and 23K the intrinsic thermal resistivity (the reciprocal of conductivity) of tantalum varied as $T^{2.0}$.

White and Woods have also investigated the electrical resistivity of 99.9% pure tantalum. They report a constant low temperature resistivity due to impurities of $2.1 \times 10^{-9} \Omega$ - m below 7K° and a smoothly increasing resistivity above this temperature. When the impurity resistivity was subtracted from the total resistivity, the resulting intrinsic resistivity varied as $T^{3.8}$ between 8K and 23K.

Jung et al. (8) have studied the transport properties of high purity vanadium, another superconducting transition metal similar to tantalum. They conclude that electrons scattering from other electrons make up a very small part of the low temperature scattering which is comprised

mostly of electron-phonon scattering. Investigation by Webb (9) of niobium, a high temperature superconducting transition metal, does not show electron-electron scattering but does exhibit strong electron-phonon scattering. The transport properties of several other transition metals which are not superconductors or very low temperature superconductors have also been investigated. Strong electron-electron scattering has been found in tungsten by Wagner et al. (10), in rhenium, palladium and osmium by Schriempf (11-13), in platinum by Anderson et al. (14) and in nickel by White and Tainish (15).

Purpose of this Research

The purpose of this research was to measure the electrical resistivity and thermal conductivity of high purity tantalum from 4.5K to 65K. The high purity (RRR up to 1714) is necessary to investigate the intrinsic electron scattering mechanisms in tantalum that have been masked at low temperatures by electron-impurity scattering in earlier work. Comparision of the results to theoretical models of the transport properties in transition metals was also done to determine if tantalum fits into the scheme of other high temperature superconducting transition metals, namely vanadium and niobium.

CHAPTER II: THEORETICAL REVIEW

The electrical conductivity of a metal (σ) is the transfer of charge by electrons. The reciprocal of the electrical conductivity is the electrical resistivity (ρ), which, according to Matthiessen's rule, can be separated into two parts

$$\rho(T) = \rho_o + \rho_i(T). \tag{1}$$

The total electrical resistivity, $\rho(T)$, is comprised of a residual electrical resistivity, ρ_o, and an intrinsic electrical resistivity, $\rho_i(T)$. To first order the residual resistivity is independent of temperature and, for a given metal, depends only on the sample purity. The intrinsic electrical resistivity is a property intrinsic to the metal and is a function of temperature.

The thermal conductivity of a metal (λ) is the conduction of energy by electrons and phonons. These two contributions add to give the total thermal conductivity, $\lambda(T)$,

$$\lambda(T) = \lambda_e(T) + \lambda_g(T), \tag{2}$$

where $\lambda_e(T)$ is the electronic thermal conductivity and $\lambda_g(T)$ is the phonon, or lattice, thermal conductivity. In good metals electrons are so mobile that, although lattice conduction is present, electron thermal conduction is by far the major contribution (16). The lattice thermal conduction in most discussions, including this one, is ignored. The reciprocal of thermal conductivity, the thermal resistivity (W), has its analog to Matthiessen's rule,

$$W(T) = W_o(T) + W_i(T). \tag{3}$$

Both the residual thermal resistivity, $W_o(T)$, and the intrinsic thermal resistivity, $W_i(T)$, are functions of temperature.

The Wiedemann-Franz-Lorenz (WFL) rule is

$$\frac{\lambda(T)}{\sigma(T)T} = L. \tag{4}$$

At low and high temperatures L, called the Lorenz ratio, is a constant,

$$L_o = \frac{\pi^2}{3}\left(\frac{k_B}{e}\right)^2 = 2.45 \times 10^{-8}\ V^2/K^2, \tag{5}$$

where k_B is the Boltzmann constant and e is the electronic charge.

The transport properties of metals have been reviewed by Wilson (17), Ziman (18), Mott (19), Lifshits et al. (20) and others.

In equilibrium, electrons in a metal are distributed in momentum space according to the well-known Fermi Dirac distribution, $f^o(\underset{\sim}{k})$,

$$f^o(\underset{\sim}{k}) = [1 + \exp\{(E(\underset{\sim}{k}) - E_F)/k_BT\}]^{-1} \tag{6}$$

where $E(\underset{\sim}{k})$ is the electron energy and E_F is the Fermi energy. Three ways in which $f(\underset{\sim}{k})$ changes with time are now considered.

External fields will exert a force on the electrons causing a time rate of change in the $\underset{\sim}{k}$-vector of each carrier.

$$\underset{\sim}{F}/\hbar = \dot{\underset{\sim}{k}} = \frac{e}{\hbar}(\underset{\sim}{E} + \underset{\sim}{v}(\underset{\sim}{k}) \times \underset{\sim}{H}). \tag{7}$$

Therefore, due to the fields, the distribution of electrons changes at the rate

$$\left.\frac{\partial f(\underset{\sim}{k})}{\partial t}\right]_{field} = -\frac{\partial \underset{\sim}{k}}{\partial t} \cdot \frac{\partial f(\underset{\sim}{k})}{\partial \underset{\sim}{k}} = -\frac{e}{\hbar}(\underset{\sim}{E} + \underset{\sim}{v}(\underset{\sim}{k}) \times \underset{\sim}{H}) \cdot \nabla_k f(\underset{\sim}{k}), \tag{8}$$

where ∇_k, the gradient in k-space, is $\frac{\partial}{\partial k}$.

The equilibrium electron distribution can also be disturbed by a temperature gradient (∇T). An electron with a velocity $\underset{\sim}{v}(\underset{\sim}{k})$ moving through a temperature gradient will experience a time rate of change of temperature.

$$\frac{\partial T}{\partial t} = \underset{\sim}{v}(\underset{\sim}{k})\cdot\nabla T. \tag{9}$$

Due to the temperature gradient, the electron distribution will change at the rate

$$\left.\frac{\partial f(\underset{\sim}{k})}{\partial t}\right]_{temp} = \frac{\partial T}{\partial t}\frac{\partial f(\underset{\sim}{k})}{\partial T} = \underset{\sim}{v}(\underset{\sim}{k})\cdot\nabla T\,\frac{\partial f(\underset{\sim}{k})}{\partial T}\,. \tag{10}$$

A third effect on the electron distribution is caused by scattering from one $\underset{\sim}{k}$ state to another. Although the effect of scattering is more complicated, by considering elastic scattering only one obtains a rate of change of $f(\underset{\sim}{k})$(17,18)

$$\left.\frac{\partial f(\underset{\sim}{k})}{\partial t}\right]_{scatt} = \int\{f(\underset{\sim}{k}')(1-f(\underset{\sim}{k})) - f(\underset{\sim}{k})(1-f(\underset{\sim}{k}'))\}Q(\underset{\sim}{k},\underset{\sim}{k}')d\underset{\sim}{k}'. \tag{11}$$

The process of scattering from $\underset{\sim}{k}$ to $\underset{\sim}{k}'$ depends on $f(\underset{\sim}{k})$, the number of carriers in state $\underset{\sim}{k}$, and $(1-f(\underset{\sim}{k}'))$, the number of vacancies in state $\underset{\sim}{k}'$. The product of these weighting functions and the basic transition probability, $Q(\underset{\sim}{k},\underset{\sim}{k}')$, gives the rate of transition from $\underset{\sim}{k}$ to $\underset{\sim}{k}'$. The competing process of a transition from $\underset{\sim}{k}'$ back to $\underset{\sim}{k}$ has the same basic transition probability and is weighted by $f(\underset{\sim}{k}')(1-f(\underset{\sim}{k}))$. These two terms are summed over all possible final scattered states $\underset{\sim}{k}'$, to give the time rate of change of $f(\underset{\sim}{k})$.

The Boltzmann equation states that for any $\underset{\sim}{k}$, at any point, the net rate of change of $f(\underset{\sim}{k})$ is zero.

$$\left.\frac{\partial f(\underset{\sim}{k})}{\partial t}\right]_{field} + \left.\frac{\partial f(\underset{\sim}{k})}{\partial t}\right]_{temp} + \left.\frac{\partial f(\underset{\sim}{k})}{\partial t}\right]_{scatt} = 0. \tag{12}$$

Using equations 8, 10, and 11 in 12 results in a linear integro-differential equation which is very difficult to solve in this form. To simplify the calculations the relaxation approximation is used for the scattering term.

$$\left.\frac{\partial f(\underset{\sim}{k})}{\partial t}\right]_{scatt} = \frac{f^{o}(\underset{\sim}{k})-f(\underset{\sim}{k})}{\tau(\underset{\sim}{k})} = \frac{-g(\underset{\sim}{k})}{\tau(\underset{\sim}{k})} . \tag{13}$$

The deviation of the electron distribution from equilibrium, $g(\underset{\sim}{k})$, and the relaxation time, $\tau(\underset{\sim}{k})$, are thus introduced. This approximation and equations 8, 10, and 12 result in the steady state condition

$$-\frac{e}{\hbar}[\underset{\sim}{E} + \underset{\sim}{v}(\underset{\sim}{k}) \times \underset{\sim}{H}]\cdot\nabla_{k} f(\underset{\sim}{k}) + \underset{\sim}{v}(\underset{\sim}{k})\cdot\nabla T \frac{\partial f(\underset{\sim}{k})}{\partial T} = \frac{g(\underset{\sim}{k})}{\tau(\underset{\sim}{k})} . \tag{14}$$

Ziman (18) states that a more advanced quantum mechanical technique using density matrices and Green functions to calculate the transport coefficients is peculiarly subtle and has only been carried out in a few simple cases. Fortunately, these confirm almost all the results obtained by the Boltzmann method.

The electric current density is

$$J = \frac{2}{(2\pi)^{3}} \int e\, \underset{\sim}{v}(\underset{\sim}{k})\, g(\underset{\sim}{k}) d\underset{\sim}{k} \tag{15}$$

integrated over all $\underset{\sim}{k}$ space.

From the definition of electrical conductivity in Ohm's law,

$$\underset{\sim}{J} = \underline{\underline{\sigma}} \cdot \underset{\sim}{E}, \tag{16}$$

it is seen that in general, $\underline{\underline{\sigma}}$ is a tensor. Wilson (17), using equations 14, 15, and 16 with $\underset{\sim}{H}$ and ∇T equal to zero, has shown

$$\sigma_{ij} = \frac{e^2}{4\pi^3} \int_{\substack{\text{Fermi} \\ \text{Surface}}} \frac{\tau_e(\underset{\sim}{k}) v_i(\underset{\sim}{k}) v_j(\underset{\sim}{k}) dS}{|\nabla_k E(\underset{\sim}{k})|} \tag{17}$$

where dS is an incremental area of the Fermi surface and v_i and v_j are the electron velocities at the Fermi energy. In an istropic, cubic metal, σ becomes a scalar,

$$\sigma = \frac{e^2}{12\pi^3} \int_{\substack{\text{Fermi} \\ \text{Surface}}} \frac{\tau_e(\underset{\sim}{k}) v(\underset{\sim}{k})^2 dS}{|\nabla_k E(\underset{\sim}{k})|} = \frac{e^2}{12\pi^2 \hbar} \int_{\substack{\text{Fermi} \\ \text{Surface}}} \bar{\ell}_e(\underset{\sim}{k}) dS, \tag{18}$$

where $\bar{\ell}_e(\underset{\sim}{k})$ is the effective mean free path for electric conduction given by $\tau_e(\underset{\sim}{k}) v(\underset{\sim}{k}) = \bar{\ell}_e(\underset{\sim}{k})$. The subscript on τ distinguishes the relaxation time for the electric current case.

The heat current density $\underset{\sim}{Q}$, is

$$\underset{\sim}{Q} = \frac{2}{(2\pi)^3} \int [E(\underset{\sim}{k}) - E_F] \underset{\sim}{v}(\underset{\sim}{k}) g(\underset{\sim}{k}) d\underset{\sim}{k} \tag{19}$$

integrated over all $\underset{\sim}{k}$ space. The thermal conductivity is defined by

$$\underset{\sim}{Q} = -\underline{\underline{\lambda}} \cdot \nabla T, \tag{20}$$

where again it is seen that $\underline{\underline{\lambda}}$ is a tensor. In a cubic metal λ becomes a scalar and, at low temperature ($k_B T << E_F$), is (17)

$$\lambda = \frac{k_B^2 T}{36\pi} \int_{\substack{\text{Fermi}\\ \text{Surface}}} \frac{\tau_\lambda(k) v^2(k) dS}{|\nabla_k E(k)|} = \frac{k_B^2 T}{36\pi} \int_{\substack{\text{Fermi}\\ \text{Surface}}} \bar{\ell}_\lambda(k) dS, \qquad (21)$$

where $\bar{\ell}_\lambda(\underset{\sim}{k})$ is the effective mean free path for thermal conduction. This is calculated from equations 14, 19, and 20 with the electric current density equal to zero.

From the similar forms for σ and λ it is easily seen that the W.F.L. rule holds if the relaxation times for electrical (τ_e) and thermal (τ_λ) conductivities are equal. At low temperatures where nearly elastic electron-phonon scattering is dominant, the electronic and thermal relaxation times are equal. However at intermediate temperatures where inelastic electron-phonon interactions are present, the W.F.L. rule does not hold.

With only an electric field and a constant temperature, equation 14 is rewritten, substituting the integral expression for the scattering term (equation 6). Ziman (17,21), assuming elastic scattering, has shown

$$\underset{\sim}{v}(\underset{\sim}{k}) \cdot \underset{\sim}{E} = \tau_e \int [\underset{\sim}{v}(\underset{\sim}{k}) - \underset{\sim}{v}(\underset{\sim}{k}')] \cdot \underset{\sim}{E}\, q(\underset{\sim}{k},\underset{\sim}{k}') d\Omega', \qquad (22)$$

where $q(\underset{\sim}{k},\underset{\sim}{k}')$ is the new scattering probability taking into account the effective electrons near the Fermi surface only, and $d\Omega'$ is an element of solid angle for the direction of $\underset{\sim}{k}'$ after scattering. With a spherical Fermi surface $q(\underset{\sim}{k},\underset{\sim}{k}')$ becomes a function of the angle between the two wavevectors only. With these conditions satisfied

$$\frac{1}{\tau_e} = \int (1-\cos\theta) q(\theta) d\Omega' . \qquad (23)$$

It is seen that the relaxation time is inversely proportional to an integral of the scattering probability but weighted by $(1-\cos\theta)$. Therefore the important thing is not that the electron was scattered, but by how much the electron's component of velocity in the direction of the electric field, is changed. Electrical conduction can be viewed as a displacement of the Fermi surface in $\underset{\sim}{k}$ space with one side of the Fermi surface gaining electrons and the other side losing electrons. A scattering event restores equilibrium by moving an electron from the excess side of the Fermi surface to the deficient side. Therefore large angle scattering (elastic), which restores the equilibrium more rapidly, is characterized by a short relaxation time.

A temperature gradient causes a change in the electron distribution by increasing the electron's energy on one side of the Fermi surface and decreasing it on the other side. Now two types of scattering become effective in restoring equilibrium. Elastic scattering, which changes the electron's direction, but not its energy, will restore equilibrium with a characteristic relaxation time depending upon the scattering angle as shown in equation 23, and the W.F.L. rule holds. Inelastic scattering, which changes the electron's energy, but not necessarily its direction, also restores equilibrium; however, there is no angular dependence in the relaxation time in this scattering,

$$\frac{1}{\tau_\lambda} = \int q(\theta) d\Omega', \tag{24}$$

and the W.F.L. rule breaks down.

Most electron-phonon scattering is inelastic at low temperatures (22). However, at temperatures low enough, the low energy phonons become ineffective in scattering and the electrical and thermal conductivities of a pure metal increase without bound as the temperature approaches zero. Ionized impurities and crystal defects can, however, restore the electron distribution. Thus, at very low temperatures, the mean free paths for electrical conductivity, equation 18, and for thermal conductivity, equation 21, are equal and depend primarily on impurities and defects and are temperature independent. The W.F.L. rule holds in this region.

As the temperature increases phonons populate higher frequencies and their scattering contribution becomes important. The general expression for electron-phonon interaction is

$$\underset{\sim}{k} + \underset{\sim}{q} = \underset{\sim}{k}' + \underset{\sim}{B}, \tag{25}$$

where $\underset{\sim}{k}$ and $\underset{\sim}{k}'$ are the initial and final electron wavevectors respectively, $\underset{\sim}{q}$ is the phonon wavevector emitted or absorbed, and $\underset{\sim}{B}$ is a reciprocal lattice vector. With $\underset{\sim}{B} = 0$ electron-phonon momentum is conserved. This normal scattering occurs at all temperatures. However, electron-phonon momentum is not conserved in Umklapp scattering where $\underset{\sim}{B} \neq 0$. U-processes occur when the phonon wavevector is greater than or equal to $\underset{\sim}{q}'$ where

$$\underset{\sim}{q}' = \underset{\sim}{B} - 2\underset{\sim}{k}_F \tag{26}$$

and $\underset{\sim}{k}_F$ is the electron Fermi wavevector. This type of scattering requires a temperature sufficiently high so that phonons are populated to wavevectors equal to or greater than $\underset{\sim}{q}'$. Klemens and Jackson (23) have shown that U-processes occur at low temperatures in metals which have Fermi surfaces which touch the Brillouin zone boundary. Umklapp processes are an important scattering mechanism since they move an electron through a large scattering angle across the Fermi surface.

The intrinsic electrical resistivity of a metal was first solved by Bloch (24). Bloch assumed normal electron-phonon scattering, a Debye phonon spectrum, a spherical Fermi surface and electrical conduction in one parabolic band. He showed that

$$\rho_i = 4A\left(\frac{T}{\theta}\right)^5 J_5, \tag{27}$$

where A is a constant proportional to the electron-phonon interaction, θ is the Debye characteristic temperature, and $J_5(\frac{\theta}{T})$ is the Debye integral for N = 5,

$$J_N\left(\frac{\theta}{T}\right) = \int_0^{\theta/T} \frac{e^x x^N \, dx}{(e^x-1)(1-e^{-x})} \tag{28}$$

At low temperatures ($T < \theta/20$), $J_5(\frac{\theta}{T})$ is a constant and

$$\rho_i(T) = 497.6A\left(\frac{T}{\theta}\right)^5. \tag{29}$$

Mott (19) in 1936, and Wilson (25) in 1938, changed Bloch's model to include electronic conduction in a normal parabolic s band and an

inverted d band that overlaps the s band in at least one direction. This is the situation in transition metals. Since the d band electrons have a much higher effective mass, any scattering event from the s to the d band would increase the electrical resistivity greatly. Mott and Wilson showed

$$\rho_i(sd) = d\left(\frac{T}{\theta}\right)^3 J_3\left(\frac{\theta}{T}\right), \tag{30}$$

where d is an electron-phonon interaction constant and

$$J_3\left(\frac{\theta}{T}\right) = \int_{\frac{\theta_{min}}{T}}^{\theta/T} \frac{e^x x^3}{(e^x-1)(1-e^{-x})}\, dx. \tag{31}$$

The constant θ_{min} is defined by

$$k_B\theta_{min} = v_o|\underset{\sim}{k}_d - \underset{\sim}{k}_s|, \tag{32}$$

where v_o is the velocity of sound and $|\underset{\sim}{k}_d - \underset{\sim}{k}_s|$ describes the minimum phonon wavevector needed to cause an s-d transition. If θ_{min} is set equal to zero the Wilson integral, equation 31, becomes a constant at temperatures below $\theta/5$ and

$$\rho_i(sd) \propto T^3. \tag{33}$$

The effect of electron-electron interactions have been examined theoretically by Baber (26) in 1937 and Pines (27,28) in 1955 and 1956. They conclude that these interactions may contribute a component of resistivity proportional to T^2 which may be appreciable at very low temperatures in some transition metals. Therefore

$$\rho_i(ee) \propto T^2. \tag{34}$$

The total expression for electrical resistivity at low temperatures, recalling Matthiessen's rule, becomes

$$\rho(T) = \rho_o + \rho_{ee}T^2 + \rho_{sd}T^3 + \rho_{ss}T^5. \tag{35}$$

The intrinsic thermal resistivity $W_i(T)$ of a metal was derived by Wilson (29) with the same assumptions as those used by Bloch. Wilson showed

$$W_i(T) = \frac{1}{\lambda_i(T)} \tag{36}$$

$$W_i(T) = \frac{4A}{L_o T}\left(\frac{T}{\theta}\right)^5 \left| \{1 + \frac{3}{2\pi^2}\frac{E_F}{D}\left(\frac{\theta}{T}\right)^2\} J_5 - \frac{1}{2\pi^2} J_7 \right|. \tag{37}$$

The constant A is proportional to the square of the electron-phonon interaction constant C, L_o is the Lorenz ratio, E_F is the Fermi energy, and

$$E_F/D = 2^{1/3}N^{2/3}, \tag{38}$$

where N is the effective number of conduction electrons per atom. Equation 37 deals with electron phonon scattering only. The first term is the thermal resistance due to elastic scattering, the second term is the thermal resistance due to inelastic scattering, and the third term is a correlation term, since these two scattering events do not act independently. At low temperatures ($T < \theta/20$) the inelastic scattering dominates and

$$W_i(T) \propto T^2. \tag{39}$$

Kemp et al. (30) have shown that both electron-phonon intraband (s-s) and interband (s-d) scattering are included in this T^2 term. Ziman (21) has shown that the electrons scatter off each other via a screened Coulomb interaction. This electron-electron scattering causes the thermal resistivity to vary linearly with T. Then equation 39 is rewritten to include both terms,

$$W_i(T) = W_{ee}T + W_{ep}T^2, \tag{40}$$

where the term $W_{ep}T^2$ contains all electron-phonon scattering. At very low temperatures the thermal conduction is limited only by scattering from impurities and crystal defects. Equation 21 shows this conduction to vary linearly with temperature where $\bar{\ell}_\lambda(\underset{\sim}{k})$ is now the mean free path for electrons between impurity and defect scattering. Therefore

$$W_o(T) = \frac{1}{\lambda_o(T)} \propto \frac{1}{T}. \tag{41}$$

The residual thermal resistance varies inversely with temperature. The thermal equivalent to Matthiessen's rule is used to combine equations 40 and 41 and this expression is multiplied by T to produce

$$WT = W_o + W_{ee}T^2 + W_{ep}T^3. \tag{42}$$

In this expression W_o is independent of temperature.

CHAPTER III: EXPERIMENTAL PROCEDURE

Sample Preparation and Characterization

The polycrystalline tantalum sample used in this research was prepared at the Ames Laboratory by F. A. Schmidt by the electrotransport technique. The electrotransport technique for purifying metals involves passing large electrical currents through cylindrical samples, causing resistive heating and impurity migration. The tantalum sample was placed in a vacuum of 3.6×10^{-10} torr and heated to 2100°C by passing a current density of 3400 A/cm^2 through it for 189 hours. Gaseous impurities are driven off because of the high vacuum and high temperature. Interstitial solutes, notably carbon, nitrogen, oxygen and hydrogen migrate to one end of the cylindrical rod due to the high current density. Details of the apparatus have been discussed by Peterson and Schmidt (31) and Peterson *et al.* (32). The interstitial impurities C, N, O, and H migrate in the direction of the applied electric field in tantalum (33) thereby causing an inpurity gradient in the direction of the electric field.

The electrotransported sample was cut into four sections of varying purity and their resistivity ratios determined. The sample characteristics are shown in Table 1.

Table 1. Sample characteristics

Section	Length (cm)	Diameter (cm)	Resistivity Ratio $\rho 298/\rho 4.2$
A	4.21	.238	666
B	4.38	.239	1052
C	4.42	.239	1714
D	4.11	.238	1345

Section D was not used in this investigation since it had a sharp rise in impurity concentration where it came in contact with the sample holder in the electrotransport apparatus.

The highest purity sample, section C, was analyzed by vacuum fusion to determine the oxygen, hydrogen and nitrogen concentrations; by combustion chromatography to determine carbon concentration and by spark source mass spectroscopy to determine the concentration of all other impurities. The results of the analysis are listed in Table 2. the largest impurities present in section C in at ppm are: H - 181, Nb - 100, C - <75, O - 57 and N - 13.

Measurement Techniques

The sample holder used in this investigation is a guarded longitudinal heat flow apparatus. It is immersed in liquid helium in a cryostat of conventional design. Although the range of temperature for this work was 4.2K to 65K, by replacing the liquid helium with liquid

Table 2. Elemental impurities in section C (in atomic ppm)

H																He
181																
Li	Be										B	C	N	O	F	Ne
1	<.01										<.3	<75	13	57	<2	<.3
Na	Mg										Al	Si	P	S	Cl	Ar
<4	<.5										<.1	<2	<.3	<.9	2	<.3
K	Ca	Sc	Ti	V	Cr	Mn	Fe	Co	Ni	Cu	Zn	Ga	Ge	As	Se	Br	Kr
<1	<.3	<.09	.9	5.8	2	<.2	2	<.1	1	1.2	<.1	<.08	<.2	<.04	<.06	<.08	<.2
Rb	Sr	Y	Zr	Nb	Mo	Tc	Ru	Rh	Pd	Ag	Cd	In	Sn	Sb	Te	I	Xe
<.02	<.1	<.5	5	100	2		<.7	<.2	<.5	<.09	<.1	<.07	<.3	<.1	<.1	<.08	<.9
Cs	Ba		Hf	Ta	W	Re	Os	Ir	Pt	Au	Hg	Tl	Pb	Bi			
<.009	<.2		<5		30	<1	<2	<1	<1	<3	<.2	<.2	<.4	<.1			
La		La	Ce	Pr	Nd	Pm	Sm	Eu	Gd	Tb	Dy	Ho	Er	Tm	Yb	Lu	
Series			<.4	<.3	<1		<.9	<.4	<2	<.5	<1	<.4	<1	<.4	<.8	<1	
Ac		Th		U													
Series		<1		<.5													

nitrogen, the temperature range is extended to room temperature. The apparatus was designed and built by W. Jung (34) and is discussed in detail in his thesis.

The electrical resistivity and thermal conductivity measurements were made with the four probe technique. Figure 1 is a schematic of the experimental technique. The samples used were cylindrical with cross sectional area A. The distance between the voltage and thermometer probes is ℓ. The temperature of the "cold" probe is T and when heat, Q, is passed through the sample, the temperature of the "hot" probe is $T + \Delta T$. The copper voltage and thermometer probes are referenced to the bath temperature (liquid helium) where they make junctions with the leads of the potentiometer. As electrical current, I, or heat current, Q, passes through the sample, ΔV is the voltage measured by the potentiometer.

Electrical resistivity measurements are made with the sample isothermal ($\Delta T = 0$). With electrical current, I, passing through the sample, the resistivity, $\rho(T)$, is

$$\rho(T) = \frac{A}{\ell} \frac{\Delta V}{I} . \tag{43}$$

Thermal conductivity measurements are made by passing heat, Q, through the sample when $I = 0$. The thermal conductivity, $\lambda(T)$, of the sample will vary between the probes as the temperature varies from $T + \Delta T$ to T. The heat current is,

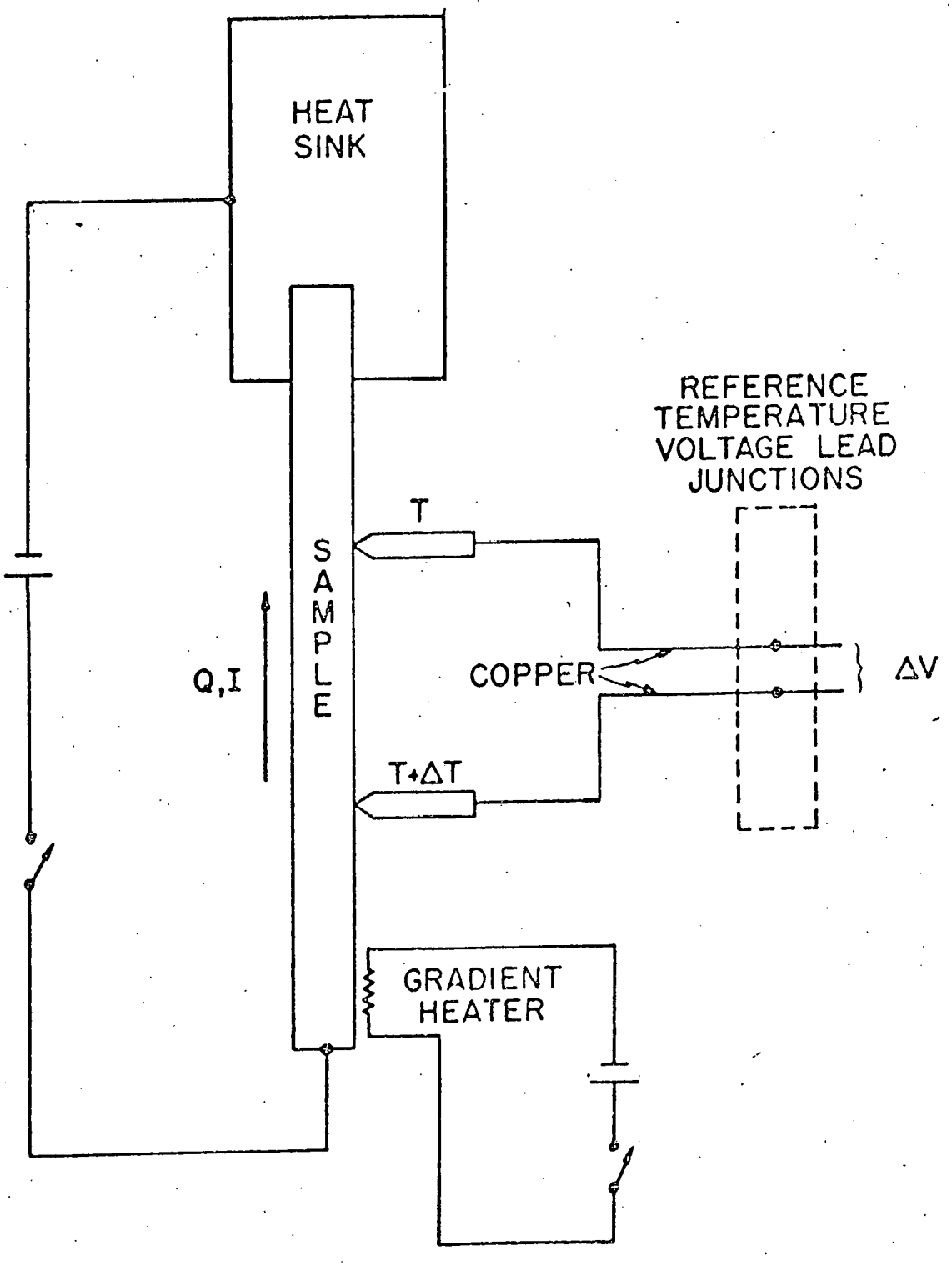

Figure 1. The four probe electrical resistivity and thermal conductivity technique.

$$Q = \frac{A}{\ell} \int_{T}^{T+\Delta T} \lambda(T')dT'. \tag{44}$$

This integral equation can be solved by expanding the thermal conductivity to first order,

$$\lambda(T') = B + CT'. \tag{45}$$

This first order expansion is good for metals at low and high temperatures if ΔT is not too large. The temperature differences between the two probes varied from .02K at low temperatures to .6K at higher temperatures for this work. With this thermal conductivity approximation the heat current is

$$Q = \frac{A}{\ell} [B + C(T + \frac{\Delta T}{2})]\Delta T \tag{46}$$

$$= \frac{A}{\ell} \lambda(T + \frac{\Delta T}{2})\Delta T. \tag{47}$$

Thus the thermal conductivity is

$$\lambda(T + \frac{1}{2} \Delta T) = \frac{\ell}{A} \frac{Q}{\Delta T} \qquad \text{for small } \Delta T. \tag{48}$$

At intermediate temperatures the thermal conductivity is a rapidly varying function of temperature and the linear approximation made in equation 45 is not valid. In this temperature region several measurements of sample temperature difference, ΔT, and heater power, Q, were made for one ambient temperature setting. The temperature gradients varied from 0.1K to 0.6K. To solve equation 44 the thermal conductivity was expanded as

$$\lambda(T) = k_1 + k_2T + k_3T^2 + \ldots + k_nT^{n-1} \tag{49}$$

where n is the number of measurements of ΔT and T vs. Q at a constant ambient temperature. The solution to the heat flow equation 44 in terms of this expansion is

$$Q = \frac{A}{\ell} \sum_{i=1}^{n} \frac{k_i}{i} [(T + \Delta T)^i - T^i]. \tag{50}$$

The n coefficients, k_i, were calculated from the n data points T and ΔT vs. Q using a least squares fit procedure. Thus at the temperature

$$T' = \frac{1}{n} \sum_{i=1}^{n} [T_i + \frac{1}{2} \Delta T_i] \tag{51}$$

the thermal conductivity is

$$\lambda(T') = \sum_{i=1}^{n} k_i (T')^{i-1}. \tag{52}$$

When n = 1 the above general expansion equals the linear expansion.

Guarded Longitudinal Heat Flow Apparatus

The low temperature measurement of electrical resistivity is difficult for two reasons. First, at low temperatures the residual resistance of the tantalum samples measured was as low as 0.25μΩ. Currents as large as 0.75A were passed through the samples in order to obtain sample voltages of 0.2μV. Since electrical resistivity is measured when the sample is isothermal, it is necessary to have large current leads anchored to the sample in order to prevent Joule heating in the current leads which would heat the sample. Secondly, in

measuring voltages in this range, minimization of thermally generated emfs is very important. The voltage clamps and leads are all constructed of the same metal, copper. Care is taken to insure that any junctions in the voltage leads are at a constant temperature.

The measurement of thermal conductivity requires that the sample gradient heater be thermally insulated from its environment. Therefore, the sample current leads for the electrical resistivity run must be removed prior to the thermal conductivity run, however the voltage and thermometer probe separation remain undisturbed. Two more difficulties arise in measuring thermal conductivity. First, it is necessary to accurately measure the ambient temperature of the sample and the sample temperature gradient. This is accomplished by the use of two chromel vs. Au - 0.03% Fe thermocouples. One absolute thermocouple measured the temperature of the "cold" thermometer clamp and was referenced to the refrigerant bath. The second differential thermocouple measured the temperature gradient between the "cold" and "hot" thermometer clamps. This was also referenced to the refrigerant bath. Secondly, all heat leaks to or from the sample must be minimized. Heat loss from radiation was minimized by the use of three radiation shields. The inner shield was constructed of stainless steel with a gradient heater at the lower end (see Figure 2). This heater produces a temperature gradient along the shield which closely matches the sample temperature gradient. Since radiative heat loss is proportional to the temperature difference between the sample and its environment, radiation

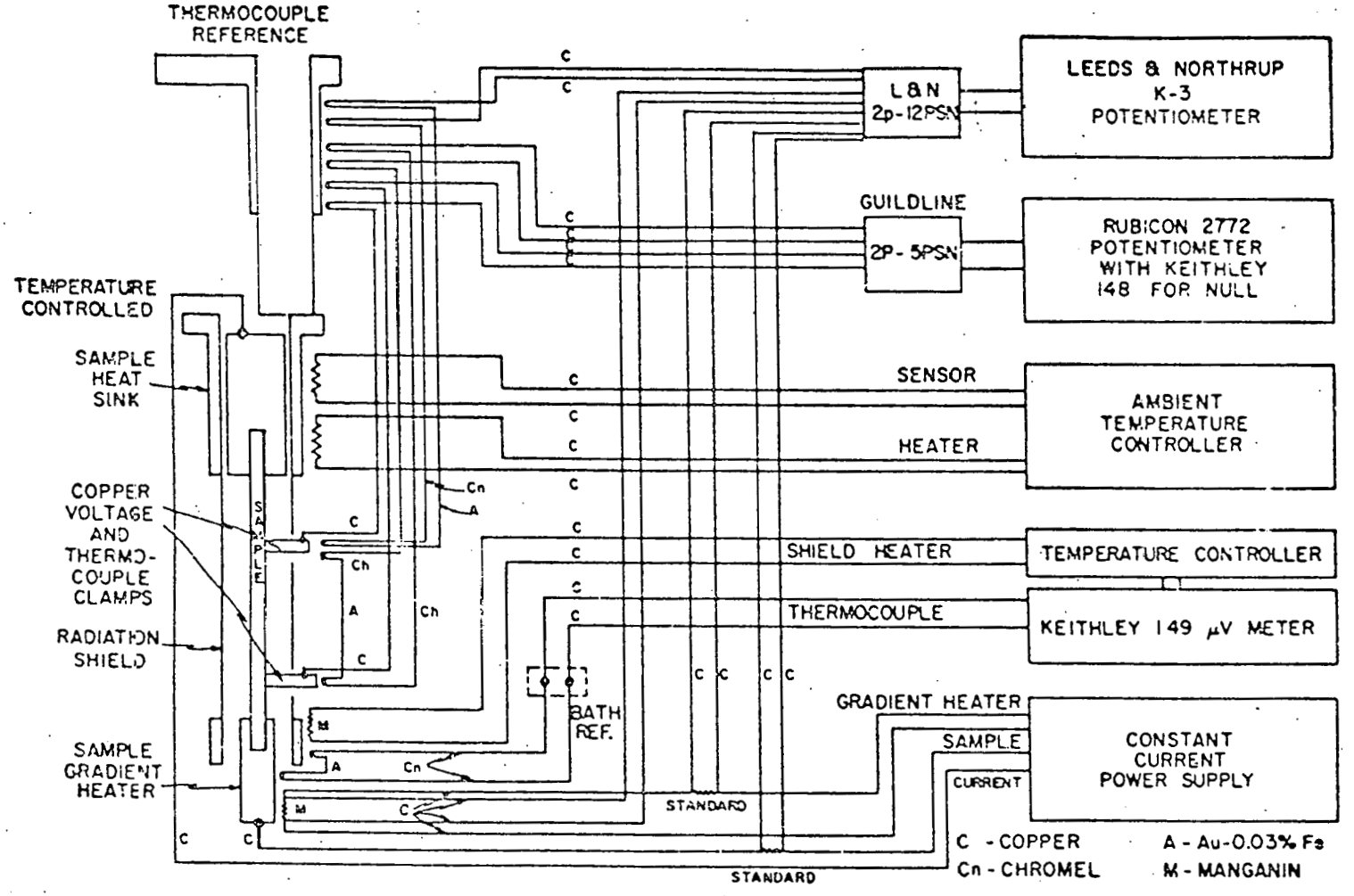

Figure 2. Schematic of sample holder with associated electronics and wiring.

loss is greatly reduced by this method. To further reduce radiated heat loss, the entire cavity between the sample and gradient radiation shield and between the gradient shield and first isothermal shield were filled with insulation. The lead wire heat loss was reduced by choosing leads of low thermal conductivity and small cross sectional area. In addition, all leads to the sample were thermally anchored to the gradient shield at positions corresponding to their locations on the sample. If the sample side of the leads are at the same temperature as the shield side, no heat will be conducted through the leads. Figure 2 shows the wiring and associated electronics. The design, construction and calibration of the apparatus are detailed by Jung (34).

Techniques for Data Taking

The form factor (voltage probe separation divided by the sample cross-sectional area) of a special sample holder was measured with a traveling microscope. The electrical resistance of each sample was then measured at liquid nitrogen temperature (77K) and the resistivity calculated. The sample was then mounted in the electrical resistivity and thermal conductivity holder and the resistance at 77K was again measured. The form factor, F, for this probe was then calculated from

$$F = \frac{R_{77K}}{\rho_{77K}} \tag{53}$$

After the sample was mounted in the holder, a #20 copper wire was soldered to the sample gradient heater and the shield gradient heater to produce a complete electrical curcuit during the electrical resistivity runs.

An a.c. temperature controller regulated the ambient temperature. The sample current was turned on after the sample reached thermal equilibrium. The approach to equilibrium could be monitored by the differential thermalcouple. The absolute thermocouple voltage, V_T, and the bath pressure, P_B, were recorded. The sample voltage, V_S, and the voltage across the standard resistor, V_{STD}, in series with the sample were recorded for both forward and reverse current directions. The resistivity of the sample was

$$\rho = \frac{1}{F} \frac{V_S(F) + V_S(R)}{V_{STD}(F) + V_{STD}(R)} R_{STD} \tag{54}$$

where R_{STD} is the resistance of the standard resistor.

The #20 Cu wire was removed from the sample during the thermal conductivity runs. The ambient sample temperature was regulated by the a.c. temperature controller and allowed to come to equilibrium. The differential thermocouple offset voltage, $V_{\Delta T}'$, and bath pressure were recorded. The shield gradient heater and sample gradient heater were turned on. After a steady state heat flow was achieved the absolute thermocouple voltage, V_T, the differential thermocouple voltage, $V_{\Delta T}$, the sample gradient heater voltage, V_H, and the sample gradient heater voltage, V_I, across the standard resistor, R_{STD}, were recorded for forward and reverse gradient heater current directions. The temperature of the "cold" thermocouple, T, was found by first calculating the reference temperature of the bath from P_B, then by using V_T and a calibrated thermocouple fit. The temperature of the sample

during the electrical resistivity runs was calculated in the same way. The sample temperature difference, ΔT, was calculated from T and $V_{\Delta T} - V_{\Delta T}'$ using the differential thermocouple fit. The thermal conductivity of the sample was

$$\lambda(T + \frac{1}{2}\Delta T) = F\frac{[V_H(F) + V_H(R)][V_I(F) + V_F(R)]}{4R_{STD}\,\Delta T} \tag{55}$$

At intermediate temperatures the thermal conductivity is calculated as shown in equations 44, 49-52.

Experimental Error

The sources of experimental error were discussed in detail by Jung (34) with the conclusion that the largest experimental uncertainty arose from measurement of the form factor. Other uncertainties are the results of temperature and temperature difference uncertainty, and sample heat loss. The maximum systematic error found by Jung was less than 3% for the thermal conductivity and 1.3% for the electrical conductivity.

The experimental uncertainty wasted by measuring the electrical resistivity and thermal conductivity of electrolytic iron, SRM734, obtained from the National Bureau of Standards. The low temperature transport properties of this material are well-documented by N.B.S.

The electrical resistivity of SRM734 is shown in Figure 3 along with the N.B.S. results. Figure 4 is a plot of the thermal conductivity of SRM734 compared to N.B.S. Figure 5 shows the percent deviation of our measurements from the N.B.S. results for the two transport properties. A systematic deviation in the low temperature electrical

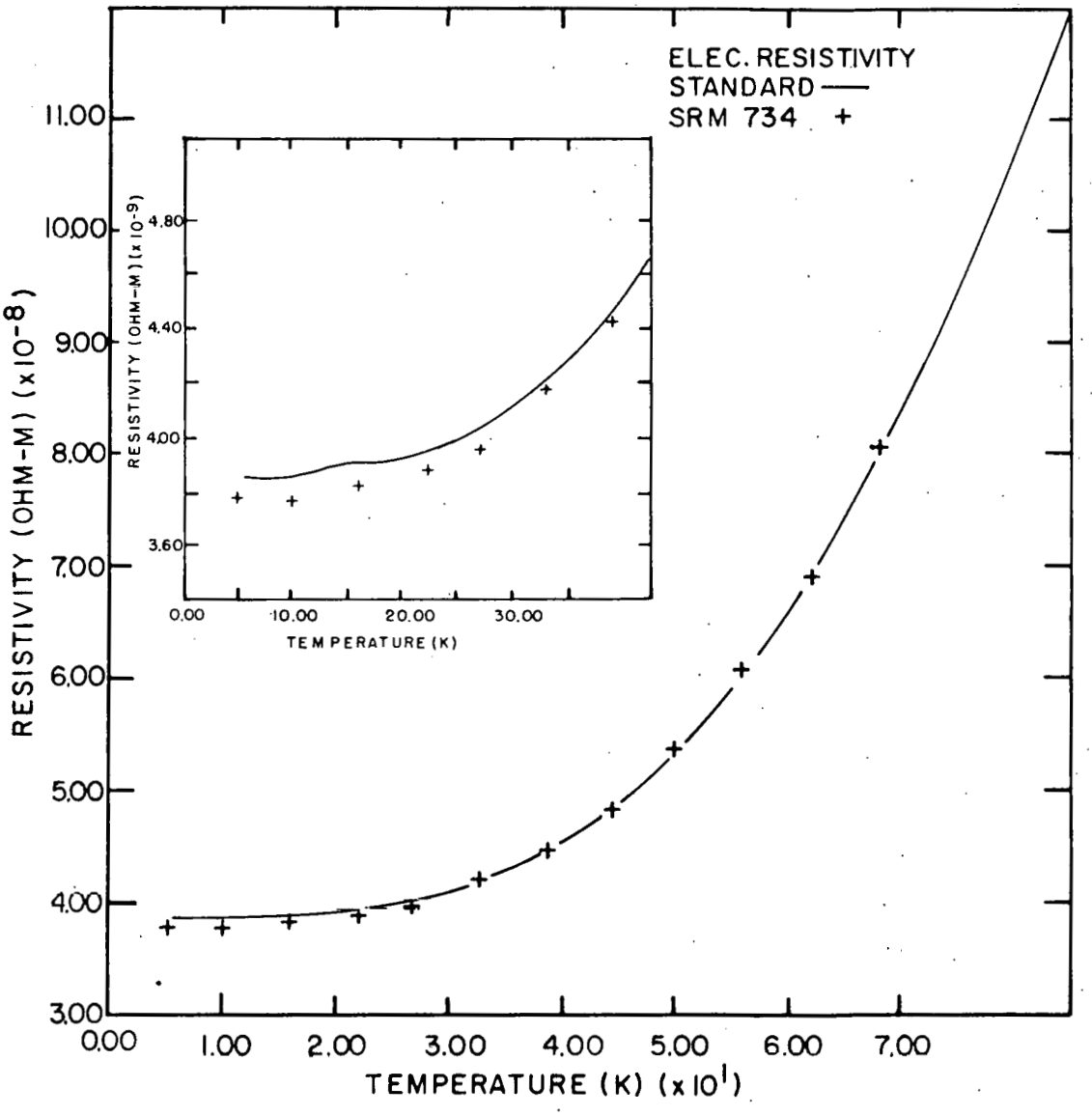

Figure 3. The electrical resistivity of SRM 734 as a function of temperature.

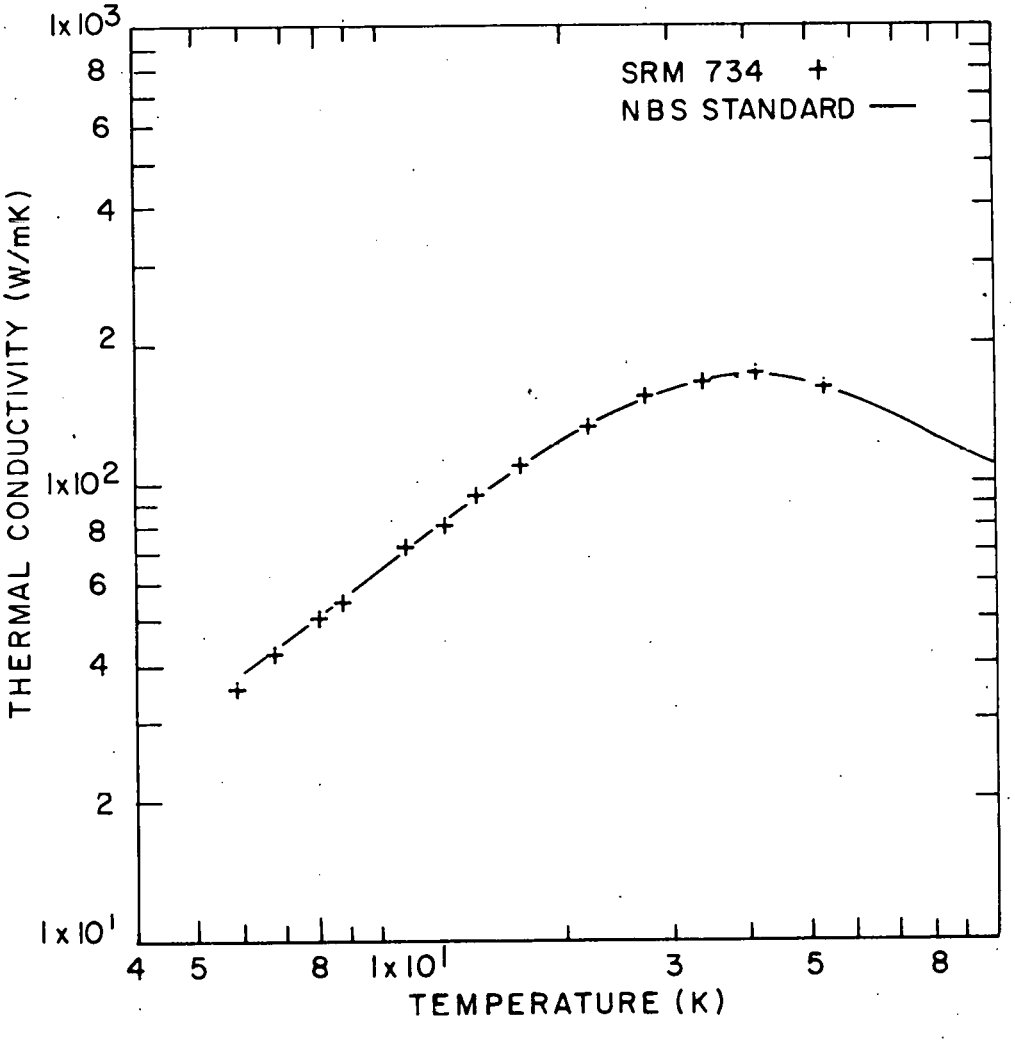

Figure 4. The thermal conductivity of SRM 734 as a function of temperature.

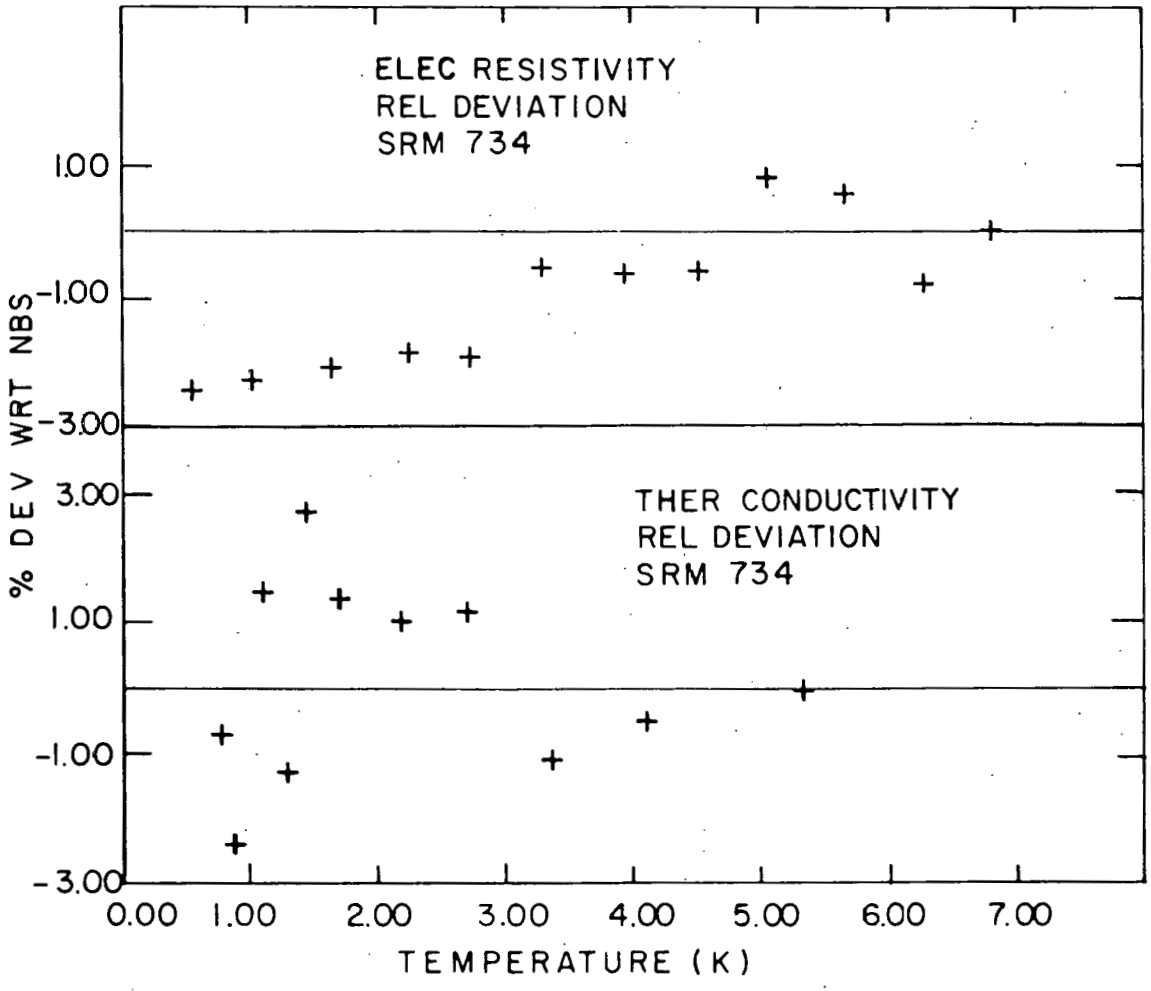

Figure 5. The percent deviation of the electrical resistivity and thermal conductivity of SRM 734 with respect to the NBS results.

resistivity of less than 3% is noted in Figure 5. The rest of the data displays random error also less than 3% for both electrical resistivity and thermal conductivity.

CHAPTER IV: RESULTS

Electrical Resistivity

Figure 6 is a plot of the electrical resistivity of tantalum as a function of temperature from 5.3K to 65K. All three samples had a smoothly varying electrical resistivity over the entire temperature range. At lower temperatures the residual resistivity became dominant with the highest purity sample, section C, exhibiting the lowest residual resistivity of $6.97 \times 10^{-11} \Omega m$. The lowest purity sample, section A, had a residual resistivity of $1.82 \times 10^{-10} \Omega m$. The fluctuation in electrical resistivity below 7K for sections A and B is believed to be caused by small time varying thermal emfs in the apparatus and do not represent any physical phenomenon. Sample voltages were read for both forward and reverse current directions, and then averaged to eliminate errors caused by thermal emfs in the apparatus. However, at low temperatures where sample voltages as low as 10 nanovolts were measured, any variation in thermal emfs between the forward and reverse current readings would have a large effect. The residual resistivity affected the total resistivity of all three samples over the entire temperature range. At each temperature, the samples of higher purity, as measured by their residual resistivity ratios (RRR), exhibited lower total electrical resistivity.

In order to separate the residual and ideal (intrinsic) resistivities, Matthiessen's rule was applied.

$$\rho_I(T) = \rho(T) - \rho_o, \tag{56}$$

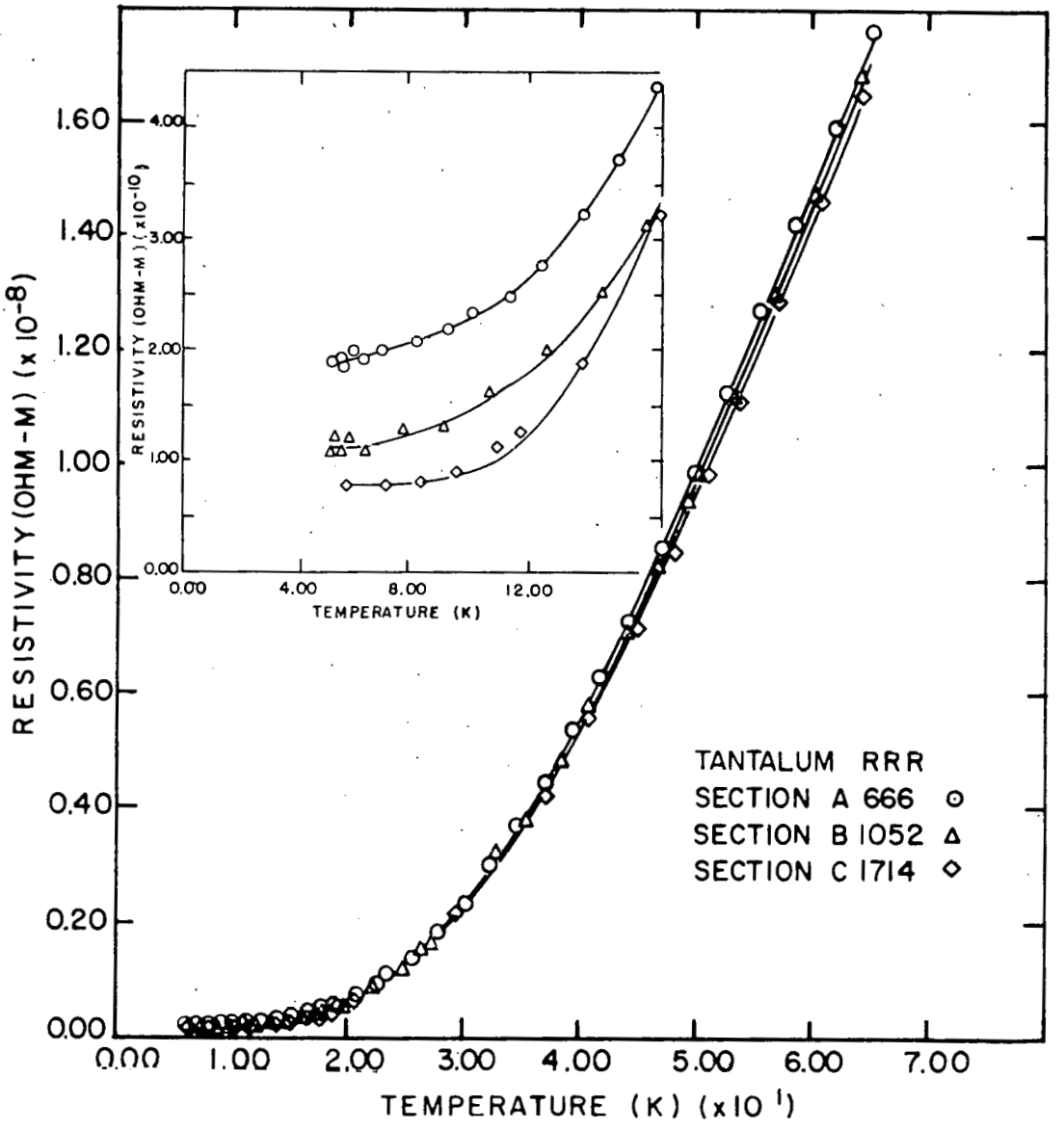

Figure 6. The electrical resistivity of tantalum as a function of temperature for three samples of high purity tantalum. The inset shows the electrical resistivity from 4.5K to 16K.

where $\rho_I(T)$ is the intrinsic electrical resistivity, $\rho(T)$ is the total resistivity and ρ_o is the residual resistivity. The residual resistivity of each sample was determined by a least squares fit program. To determine the temperature dependence of the intrinsic electrical resistivity, a plot of log ρ_I vs. log (T) was made as shown in Figure 7. As seen in this plot, the ideal resistivity varied as $T^{3.9}$ between 10K and 31K. White and Woods (3) made a similar analysis of a lower purity tantalum sample with a resistivity ratio of 62.1. They report a $T^{3.8}$ temperature dependence between 8K and 23K. All three samples had nearly identical intrinsic electrical resistivities indicating that the differences in total electrical resistivities over this temperature range were due to point impurity scattering. The scatter of points below 10K is the result of subtracting terms of nearly equal value in evaluating ρ_I.

Thermal Conductivity

The thermal conductivity of tantalum as a function of temperature is plotted in Figure 8. As can be seen in the figure, the three samples had quite similar thermal conductivities above 22K with the highest purity sample, section C, exhibiting a slightly higher conductivity. At lower temperatures a maximum is shown. Both the height and position of this maximum varied with sample purity. The lowest purity sample, section A, had the smallest maximum occurring at the highest temperature. Sections B and C had nearly equal thermal conductivity maximums of 828 W/mk at about 10K. Earlier investigations of less pure tantalum by

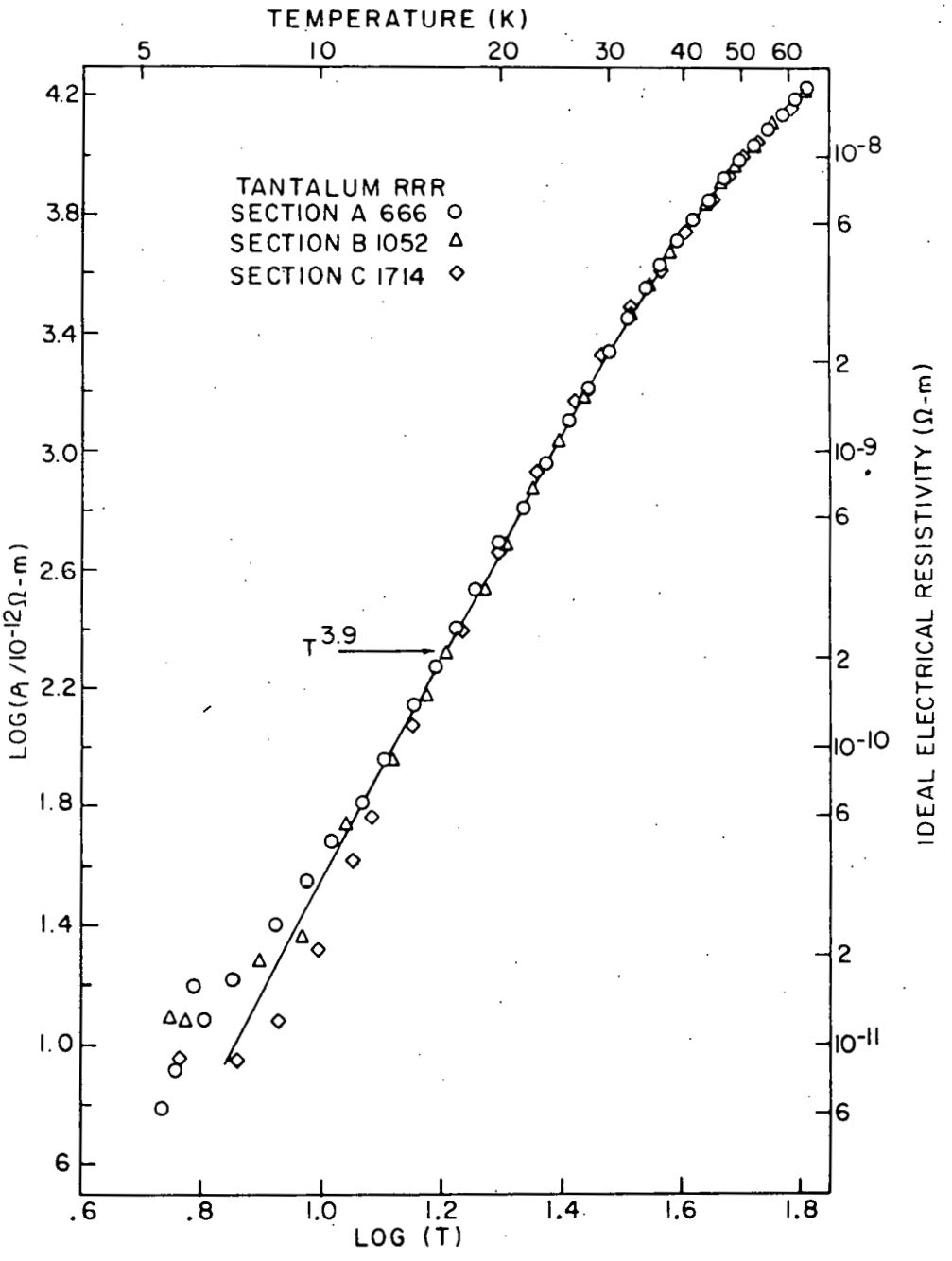

Figure 7. The log of the ideal electrical resistivity of tantalum as a function of the log of the temperature. The ideal electrical resistivity varied as $T^{3.9}$ from 10K to 31K.

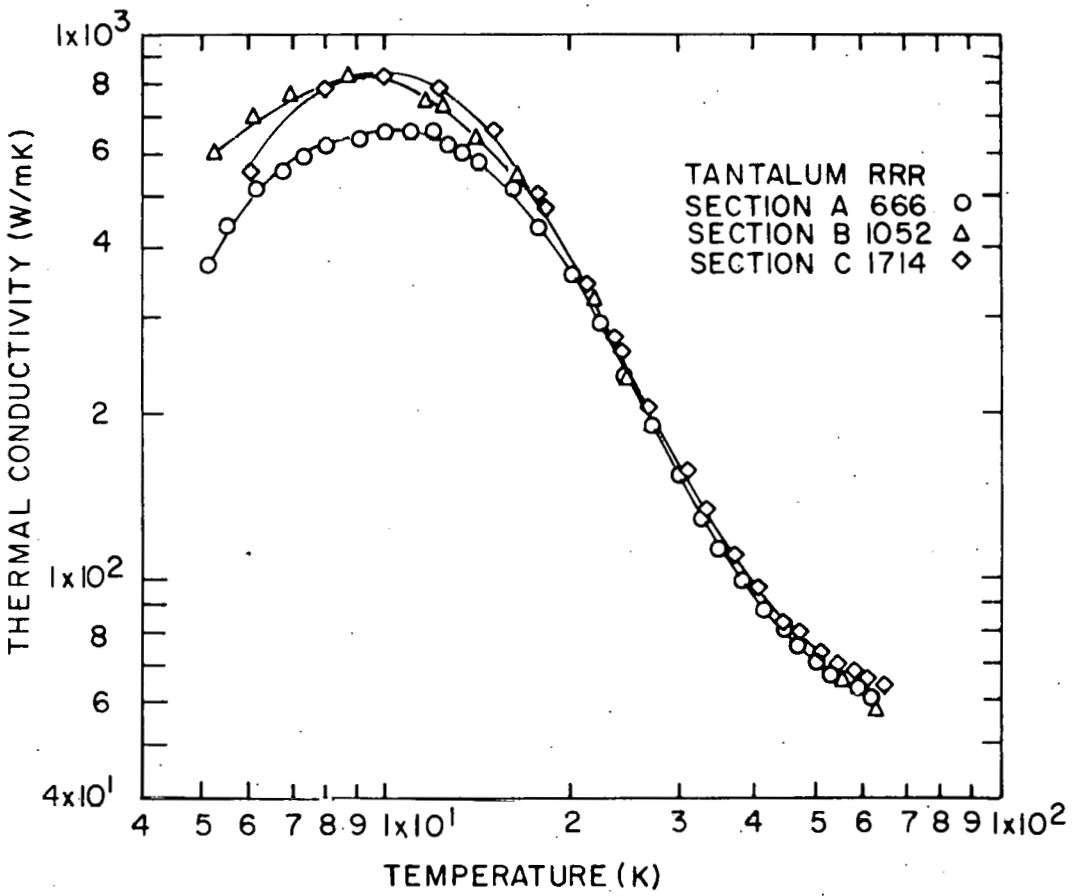

Figure 8. The thermal conductivity of tantalum as a function of temperature for three samples of high purity tantalum.

White and Woods (3) shows a maximum in thermal conductivity at 21K, but only 18% as great as that of section C.

The thermal equivalent of Matthiessen's rule was applied to the thermal resistivity.

$$W_I(T) = W(T) - W_o/T, \tag{57}$$

where $W_I(T)$ is the intrinsic thermal resistivity, W(T) is the total resistivity and W_o/T is the resistivity caused by point impurity scattering. To determine the impurity constant W_o for each sample, the expression

$$[W(T)]T = [W_I(T)]T + W_o \tag{58}$$

was least squares fit to temperature. Section B had the smallest impurity constant of $7.42 \times 10^{-3} mK^2/W$. The temperature dependence of the intrinsic thermal resistivity was determined by plotting log W_I vs. log T as shown in Figure 9. Again, a scattering of points below 10K results from subtracting terms of nearly equal value. From 10K to 35K the intrinsic thermal resistivities of all three samples are nearly identical and exhibit a $T^{2.4}$ temperature dependence. This value is greater than the $T^{2.0}$ temperature dependence reported by Powell and Blanpied (7) between 8K and 23K.

Lorenz Ratio

The Lorenz ratio of tantalum as a function of temperature is plotted in Figure 10. The low temperature region of these curves vary widely between samples. The Lorenz ratio can be determined by multiplying the thermal conductivity by the electrical resistivity at one

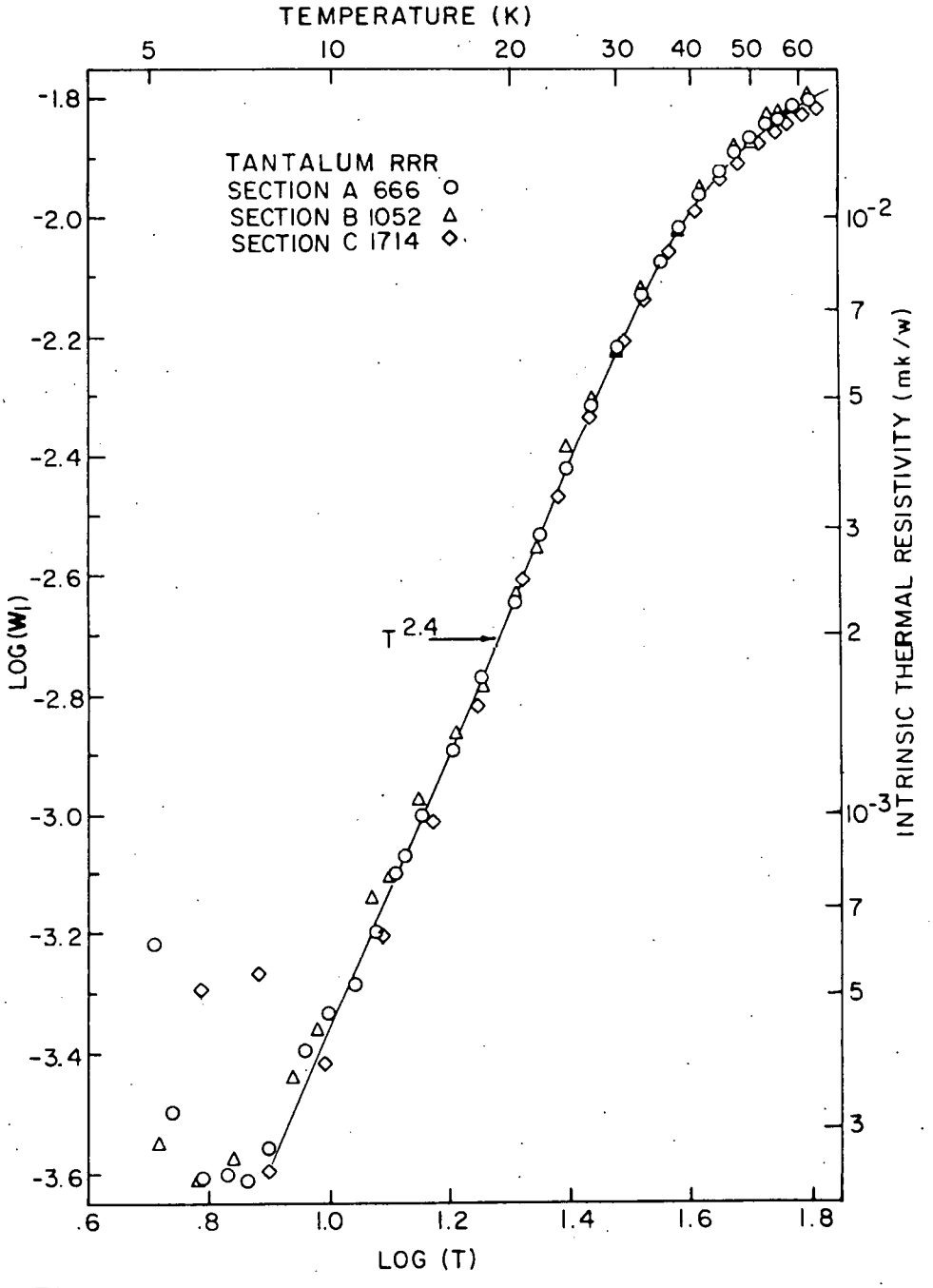

Figure 9. The log of the intrinsic thermal resistivity of tantalum as a function of the log of the temperature. The intrinsic thermal resistivity varied as $T^{2.4}$ from 10K to 35K.

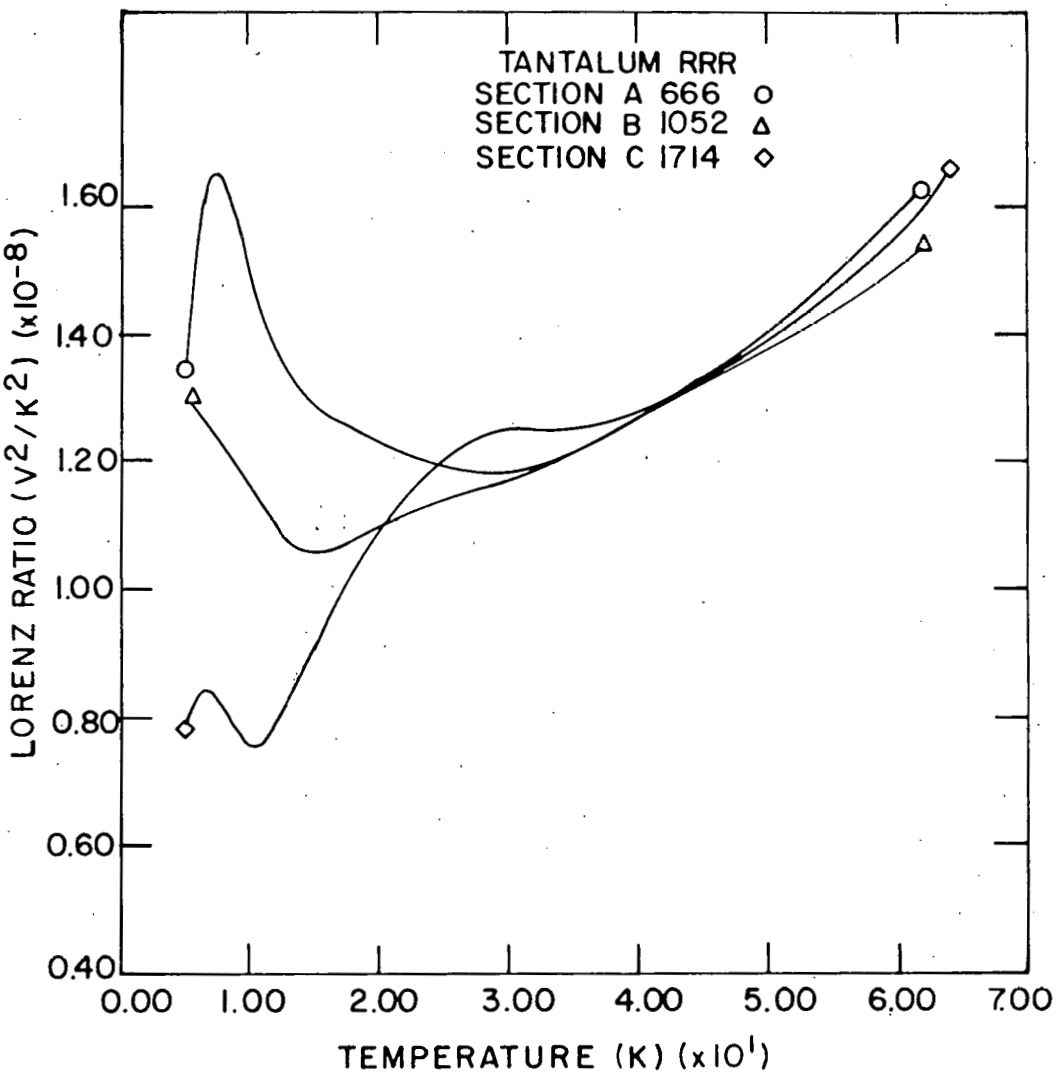

Figure 10. The Lorenz ratio of tantalum as a function of temperature. The Lorenz ratio had a low temperature minimum which was purity dependent. The Lorenz ratio was less than the Sommerfeld value over the entire temperature range.

temperature then dividing by that temperature. Since the thermal conductivity is an extremely rapidly varying function at low temperatures, the erratic behavior of the left hand tails of the curves is not surprising. However, Figure 10 has three important features. First, at low to intermediate temperatures, a minimum in the Lorenz ratio is observed due to inelastic electron-phonon scattering. This minimum is dependent on sample purity. The highest purity sample had a minimum of 0.76 V^2/K^2 at 10.5K. As the purity of the samples decreased, the minimum became less pronounced and its position shifted to higher temperatures. Secondly, as the temperature increased and elastic electron-phonon scattering became more dominant, the Lorenz ratios of the three samples converged. This occurred at temperatures greater than 40K. Thirdly, the Lorenz ratio of all three samples was less than the Sommerfeld value ($L_o = 2.45 \times 10^{-8}\ V^2/K^2$) over the entire temperature range, but as the temperature increased and the three curves converged, the Lorenz ratio increased toward the Sommerfeld value.

CHAPTER V: DISCUSSION

Thermal Conductivity

At low temperatures the expression for thermal resistivity (the reciprocal of conductivity) was shown to be

$$W(T) = W_o/T + W_{ee}T + W_{ep}T^2. \tag{59}$$

The residual thermal resistivity (W_o/T) is caused by electrons scattering from impurities and has a T^{-1} temperature dependence as shown by Wilson (17). The electron-electron resistivity contribution ($W_{ee}T$) was shown to vary linearly with temperature by Ziman (21). The electron-phonon term ($W_{ep}T^2$) contains the effects of interband and intraband scattering both of which possess a T^2 temperature dependence according to Kemp et al. (30).

The total electronic thermal resistivity times temperature was represented by the equation

$$[W(T)]T = W_o + W_{ee}T^2 + W_{ep}T^3. \tag{60}$$

The thermal resistivity data was least squares fit to three different expressions representing all possible combinations of terms in equation 60 for each sample. The least squares fit to a polynomial computer program was modeled after Bevington (35). The program calculated the coefficients of the specified polynomial by minimizing χ^2, the goodness of fit to the data. No weighting factor was used with the data. A root-mean-square percent deviation was also generated for each fit. Since the data spanned several orders of magnitude it was felt that a

percent deviation for each point would give a more accurate measure of fit than an absolute deviation which would place more emphasis on the lower temperature points. The program also shows the percent error of each point from the best fit function. The results are shown in Table 3 along with the temperature range of the data and the rms percent deviation for each expression.

It is assumed that all temperature coefficients are positive, corresponding to a real physical contribution. With this restriction, the best possible fit of the data to the model used is obtained by representing the thermal resistivity times temperature by

$$WT = W_o + W_{ep}T^3. \tag{61}$$

In comparing each point to this best fit expression it is seen that the scatter is not completely random indicating that another term in equation 61 may be needed to fit the data more accurately. A contribution from Umklapp scattering may be helpful. However, no further reductions of the rms percent deviation is obtained by including the electron-electron scattering term since this fit results in a unphysical negative W_{ee}. Representing the intrinsic thermal resistivity by the electron-electron term alone produces a much larger percent deviation for each sample and very pronounced systematic scattering of points. The large value for W_U for section C is disturbing and probably results from the small number of points analyzed. These results would seem to indicate that the dominant scattering process determining the low temperature intrinsic thermal resistivity of tantalum is electron-phonon

Table 3. The coefficients W_o, W_{ee} and W_{ep} for various expressions for the thermal resistivity times temperature of tantalum. The rms percent deviation for each fit is included

Resistivity times Temp, WT	RMS Percent Deviation	W_o $\times 10^{-2}$ m-k^2/W	W_{ee} $\times 10^{-4}$ m/W	W_{ep} $\times 10^{-5}$ m/K-W
SECTION A 5.5k - 21.6k				
$W_o + W_{ee}T^2$	11.99	0.669	0.990	
$W_o + W_{ep}T^3$	4.18	1.04		0.525
$W_o + W_{ee}T^2 + W_{ep}T^3$	1.35	1.23	-0.495	0.776
SECTION B 5.4k - 20.3k				
$W_o + W_{ee}T^2$	14.38	0.389	0.016	
$W_o + W_{ep}T^3$	3.86	0.742		0.533
$W_o + W_{ee}T^2 + W_{ep}T^3$	2.27	0.859	-0.313	0.691
SECTION C 5.8k - 20.1k				
$W_o + W_{ee}T^2$	21.19	0.410	1.026	
$W_o + W_{ep}T^3$	11.89	0.817		0.515
$W_o + W_{ee}T^2 + W_{ep}T^3$	5.04	1.307	-1.132	1.054

scattering. Since both interband and intraband scattering have the same temperature dependence, nothing can be said about the relative contributions of each term from this data alone.

Electrical Resistivity

At low temperatures the expression for the total electrical resistivity of a transition metal due to normal processes was shown to be

$$\rho(T) = \rho_o + \rho_{ee}T^2 + \rho_{sd}T^3 + \rho_{ss}T^5. \tag{62}$$

The residual electrical resistivity (ρ_o) is due to scattering of electrons by impurities and other point defects. Matthiessen's rule states that this impurity term is independent of temperature and independent of the other scattering terms. The second term ($\rho_{ee}T^2$) is the resistivity caused by electrons scattering from other electrons. The T^2 temperature dependence is predicted by Baber (26) and Pines (27,28). Electrons scattered by phonons with the electrons remaining in the parabolic s conduction band give rise to the $\rho_{ss}T^5$ contribution to the total electrical resistivity as predicted by Bloch (24). Mott (19) and Wilson (25) have shown that conduction can occur in both the normal s band and in the d band typical of transition metals.

$$\sigma = \frac{n_s e^2}{m_s^*}\tau_s + \frac{n_d e^2}{m_d^*}\tau_d \tag{63}$$

where m_s^* and m_d^* are the electron effective masses in the s and d bands, n_s and n_d are the electron concentrations in the s and d bands and τ_s and τ_d are the electron relaxation times for the s and d bands.

Mott argued that, in transition metals, conductivity in the s band is much greater than conductivity in the d band due to the small effective mass of the s band electrons. Therefore, an electron-phonon interaction which scatters the electron from the s to the d band traps the electron in the high resistivity band and increases the total resistivity. Wilson has shown that s to d band transitions can occur if the phonon wavevector is larger than the difference in wavevectors of the s and d band electrons.

$$\underset{\sim}{q} > |\underset{\sim}{k}_d - \underset{\sim}{k}_s|. \tag{64}$$

Band calculations by Petroff and Viswanathan (36) have shown that the s and d bands of tantalum overlap at the Fermi surface in some regions. Therefore a very low energy phonon will cause an s to d band transition and this contribution to the total resistivity will be present at low temperatures. This interband electron-phonon process varies at T^3 according to Wilson.

For each sample, seven different expressions for the electrical resistivity, representing all possible combinations of the terms in equation 62, was fit to the data. The results are shown in Table 4 along with the temperature range of the data.

It is assumed that all temperature coefficients in equation 62 are positive, therefore any polynomial with negative coefficients represent an unphysical fit and will be ignored. It is seen from Table 4 that using ρ_{ee}, ρ_{sd} or ρ_{ss} separately produces the worst fit for each sample with the electron-electron term alone being the worst

Table 4. The coefficients ρ_o, ρ_{ee}, ρ_{sd} and ρ_{ss} for various expressions for the electrical resistivity of tantalum. The rms percent deviation for each fit is included

Resistivity, ρ	RMS Percent Deviation	ρ_o $\times 10^{-10}$ Ω-m	ρ_{ee} $\times 10^{-12}$ Ω-m/k^2	ρ_{sd} $\times 10^{-13}$ Ω-m/k^3	ρ_{ss} $\times 10^{-16}$ Ω-m/k^5
SECTION A 5.5k - 21.6k					
$\rho_o + \rho_{ee}T^2$	9.59	1.38	1.07		
$\rho_o + \rho_{sd}T^3$	4.29	1.72		0.576	
$\rho_o + \rho_{ss}T^5$	5.08	2.00			1.66
$\rho_o + \rho_{ee}T^2 + \rho_{sd}T^3$	2.01	2.00	-0.795	0.987	
$\rho_o + \rho_{ee}T^2 + \rho_{ss}T^5$	1.26	1.77	0.370		1.14
$\rho_o + \rho_{sd}T^3 + \rho_{ss}T^5$	1.28	1.84		0.306	0.803
$\rho_o + \rho_{ee}T^2 + \rho_{sd}T^3 + \rho_{ss}T^5$	1.23	1.81	0.171	0.165	0.958

Table 4. (continued)

Resistivity, ρ	RMS Percent Deviation	ρ_o $\times 10^{-10}$ Ω-m	ρ_{ee} $\times 10^{-12}$ Ω-m/k^2	ρ_{sd} $\times 10^{-13}$ Ω-m/k^3	ρ_{ss} $\times 10^{-16}$ Ω-m/k^5
SECTION B 5.4k - 20.3k					
$\rho_o + \rho_{ee}T^2$	14.10	0.665	0.993		
$\rho_o + \rho_{sd}T^3$	6.92	0.962		0.530	
$\rho_o + \rho_{ss}T^5$	7.91	1.180			1.470
$\rho_o + \rho_{ee}T^2 + \rho_{sd}T^3$	4.27	1.210	-0.753	0.914	
$\rho_o + \rho_{ee}T^2 + \rho_{ss}T^5$	3.79	0.997	0.330		1.030
$\rho_o + \rho_{sd}T^3 + \rho_{ss}T^5$	3.74	1.060		0.271	0.740
$\rho_o + \rho_{ee}T^2 + \rho_{sd}T^3 + \rho_{ss}T^5$	3.74	1.030	-0.186	0.120	0.903

Table 4. (continued)

Resistivity, ρ	RMS Percent Deviation	ρ_o $\times 10^{-10}\ \Omega$-m	ρ_{ee} $\times 10^{-12}\ \Omega$-m/k^2	ρ_{sd} $\times 10^{-13}\ \Omega$-m/k^3	ρ_{ss} $\times 10^{-16}\ \Omega$-m/k^5
SECTION C 5.8k - 20.1k					
$\rho_o + \rho_{ee}T^2$	35.69	0.015	1.115		
$\rho_o + \rho_{sd}T^3$	15.46	0.453		0.571	
$\rho_o + \rho_{ss}T^5$	5.57	0.803			1.533
$\rho_o + \rho_{ee}T^2 + \rho_{sd}T^3$	2.19	0.991	-1.248	1.180	
$\rho_o + \rho_{ee}T^2 + \rho_{ss}T^5$	3.90	0.657	0.192		1.299
$\rho_o + \rho_{sd}T^3 + \rho_{ss}T^5$	3.45	0.697		0.164	1.111
$\rho_o + \rho_{ee}T^2 + \rho_{sd}T^3 + \rho_{ss}T^5$	2.06	0.864	-0.689	0.716	0.521

fit of the three. In each case the scatter of points was systematic indicating the need for another term. The combination of electron-electron scattering and interband (s-d) electron-phonon scattering produced a negative ρ_{ee} for each sample. The inclusion of all three scattering terms results in negative electron-electron coefficients in sections B and C. In section A the rms percent deviation did not decrease significantly below the deviation for the $\rho_{ee}-\rho_{ss}$ and $\rho_{ee}-\rho_{sd}$ fits as might be expected with the inclusion of an extra degree of freedom in the least squares fit. The focus, therefore, falls on two expressions for the resistivity: the electron-electron term in combination with the intraband term and the interband term together with the intraband term. Neither expression has a significantly lower deviation for any of the sections. The scatter of points with respect to the fitted curve is random for both expressions for all three sections. The $\rho_{ee}-\rho_{ss}$ fit for section A appears to have a small systematic scatter from 12K to 21K. On the basis of this analysis alone it is very difficult to determine the best expression; however, the thermal conductivity analysis indicated that electron-electron scattering plays a very small role in low temperature transport properties of tantalum. On the basis of this result and the above analysis it is suggested that the electrical resistivity is best represented by

$$\rho = \rho_o + \rho_{sd}T^3 + \rho_{ss}T^5. \tag{65}$$

Table 5 shows the coefficients for the best fit for each section.

Table 5. The coefficients ρ_o, ρ_{sd} and ρ_{ss} of the electrical resistivity of tantalum; $\rho = \rho_o + \rho_{sd}T^3 + \rho_{ss}T^5$

SECTION	A	B	C
ρ_o ($x10^{-10}\Omega$-m)	1.84	1.06	0.697
ρ_{sd} ($x10^{-13}\Omega$-m/K^3)	0.306	0.271	0.164
ρ_{ss} ($x10^{-16}\Omega$-m/K^5	0.803	0.740	1.11

As sample purity increases the electrical resistivity contribution from interband (s-d) electron-phonon scattering is seen to decrease while the intraband (s-s) contribution becomes more dominant. At 5K interband scattering is responsible for 94% of the intrinsic resistivity of the least pure sample while interband scattering accounts for only 86% of the intrinsic resistivity of the most pure sample. At 20K the interband contributions fall to 49% for the least pure sample and 27% for the most pure sample. The remainder of the intrinsic resistivity in each case is due to the intraband electron-phonon scattering in accord with Matthiessen's rule.

$$\rho(T) = \rho_o + \rho_I(T) \tag{66}$$

where

$$\rho_I(T) = \rho_{sd}T^3 + \rho_{ss}T^5 \tag{67}$$

Using the coefficients listed in Table 5 at any given temperature, it

is seen that the total intrinsic resistivity decreases as sample purity increases. This purity dependent intrinsic resistivity is a departure from Matthiessen's rule. Similar variations of ρ_I with sample purity have been observed in other metals and recently in potassium by Newrock and Maxfield (37) and in vanadium by Jung et al. (8). Bass (38) has written a comprehensive review of deviations from Matthiessen's rule (DMR). He proposes several physical mechanisms as sources of DMR. They include:

(1) Changes in the Fermi surface, electronic wavefunctions or electronic structure upon addition of impurities.

(2) Changes in the effective number of electrons upon addition of impurities.

(3) Changes in the phonon spectrum due to differences between the average masses or force constants of the impurities and host metal.

(4) 'Quasi-local modes' in the phonon spectrum with the addition of heavy impurities.

(5) Inelastic electron-impurity scattering.

(6) Anisotropic electron-impurity scattering due to anisotropy of the impurity potential.

Petroff and Viswanathan's investigation (36) of the band structure of tantalum revealed a crossing of the s and d bands at 0.5 ev below the Fermi energy and a critical point in the s band at the Fermi energy. Scattering phenomenon associated with these two regions are very

sensitive to any change in the Fermi energy such as those suggested by (1) and (2) above.

The relaxation times for s to d band electron-phonon scattering are the same for electrical and thermal conduction (17,30), thus the interband scattering term for thermal resistivity ($W_{sd}(T)$) and for electrical resistivity ($\rho_{sd}T^3$) are related by the WFL rule.

$$W_{sd}(T) = \frac{\rho_{sd}}{L_o} T^2. \tag{68}$$

Thus, by this method, the intrinsic thermal resistivity can be separated into interband and intraband contributions.

$$W_I(T) = (W_{ss} + W_{sd})T^2. \tag{69}$$

Table 6 shows the coefficients for the best fit of the thermal resistivity data for each sample.

Table 6. The coefficients W_o, W_{ss} and W_{sd} of the thermal resistivity of tantalum; $W = W_o/T + (W_{ss} + W_{sd})T^2$

SECTION	A	B	C
W_o ($x10^{-2}$ m - K^2/W)	1.04	0.742	0.817
W_{ss} ($x10^{-6}$ m/K - W)	4.00	4.22	4.48
W_{sd} ($x10^{-6}$ m/K - W)	1.25	1.11	0.669

The total intrinsic thermal resistivity remains fairly constant as sample purity changes; but similar to the electrical resistivity case, intraband s-s scattering becomes more favored at the expense of interband s-d electron-phonon scattering as sample purity is increased. In the purest sample, interband scattering accounts for only 13% of the total intrinsic resistivity.

Tantalum appears to fit the pattern of niobium and vanadium all of which are good superconducting transition metals. For all three metals the strong electron-phonon interaction and weak electron-electron interaction (9,34) are undoubtedly related to their high superconducting transition temperatures. Other transition metals which are not superconductors or very low temperature superconductors such as tungsten, rhenium, palladium, osmium, platinum and nickel show strong electron-electron scattering (9-15).

CHAPTER VI: SUMMARY

The thermal and electrical conductivities of high purity tantalum from 5K to 23K were limited by impurity electron scattering and electron-phonon interactions. In addition to the normal s-band electron-phonon interactions, interband electron scattering between the s and d bands were also observed. There was no evidence of electron-electron scattering in this temperature range. The thermal conductivity data however, didn't fit the proposed model exactly, leaving room perhaps, for another scattering mechanism. Deviations from Matthiesen's rule were also observed in this temperature range. The Lorenz ratio was less than the Sommerfeld value over the entire temperature range. A minimum in the Lorenz ratio was observed in each sample owing to inelastic electron-phonon scattering.

Tantalum, with a superconducting transition temperature of 4.48K, is consistent in its lack of electron-electron scattering with two other superconducting transition metals: vanadium and niobium. Most normal transition metals exhibit strong electron-electron scattering.

LITERATURE CITED

1. Hammond, C. R., in Handbook of Chemistry and Physics, edited by R. C. Weast, (The Chemical Rubber Company, Cleveland, 1972), p. B-32.

2. Von Bolton, W., in Kirk-Othmer Encyclopedia of Chemical Technology, edited by A. Standen, (John Wiley and Sons, New York, 1970), vol. 19, p. 630.

3. White, G. K. and Woods, S. B., Phil. Trans. R. Soc. 251, 273 (1959).

4. Killean, R. C. G. and Lisher, E. J., J. Phys. C 8, 3510 (1975).

5. Mendelssohn, K. and Olson J. L., Proc. Phys. Soc. A 63, 1182 (1950).

6. Mendelssohn, K. and Rosenberg, H. M., Proc. Phys. Soc. A 65, 388 (1952).

7. Powell, R. L. and Blanpied, W. A., NBS Circular 556, (1954).

8. Jung, W. D., Schmidt, F. A. and Danielson, G. C., Phys. Rev. B 15, 659 (1977).

9. Webb, G. W., Phys. Rev. B 181, 1127 (1969).

10. Wagner, D. K., Garland, J. C. and Bowers, R., Phys. Rev. B 3, 3141 (1971).

11. Schriempf, J. T., J. Phys. Chem. Solids 28, 2581 (1967).

12. Schriempf, J. T., Phys. Rev. Lett. 19, 1131 (1967).

13. Schriempf, J. T., Solid State Commun. 6, 873 (1968).

14. Anderson, A. C., Peterson, R. E. and Robichaux, J. E., Phys. Rev. Lett. 20, 459 (1968).

15. White, G. K. and Tainish, R. J., Phys. Rev. Lett. 19, 165 (1967).

16. Klemens, P. G., in Handbuch der Physik, edited by S. Flügge, (Springer-Verlag, Berlin, 1956), vol. 14, p. 198.

17. Wilson, A. H., The Theory of Metals, (Cambridge University Press, London, 1953).

18. Ziman, J. M., Principles of the Theory of Solids, (Cambridge University Press, New York, 1972).

19. Mott, N. F., Proc. Roy. Soc. A 153, 699 (1936).

20. Lifshits, I. M., Azbel´, M. Ya and Kagonov, M. I., Electron Theory of Metals, (Consultants Bureau, New York-London, 1973).

21. Ziman, J. M., Electrons and Phonons, (Oxford Univeristy Press, London, 1960).

22. Klemens, P. G., in Thermal Conductivity, edited by R. P. Tye, (Academic Press, New York, 1969), vol. 1, p. 1.

23. Klemens, P. G. and Jackson, J. L., Physica 30, 2031 (1964).

24. Bloch, F., Z. Phys. 59, 208 (1930).

25. Wilson, A. H., Proc. Roy. Soc. A 167, 580 (1938).

26. Baber, W. G., Proc. Roy. Soc. A 158, 383 (1937).

27. Pines, D., Solid State Physics, 1, (Academic Press, New York, 1955).

28. Pines, D., Canad. J. Phys. 34, 1379 (1956).

29. Wilson, A. H., Proc. Camb. Phil. Soc. 33, 371 (1937).

30. Kemp, W. R. G., Klemens, P. G., Sreedhar, A. K. and White, G. K., Phil. Mag. 46, 811 (1955).

31. Peterson, D. T. and Schmidt, F. A., J. Less-Common Metals 24, 223 (1971).

32. Peterson, D. T., Schmidt, F. A. and Verhoven, J. D., Trans. Metall. Soc. A.I.M.E. 236, 1311 (1966).

33. Schmidt, F. A. and Carlson, O. N., J. Less-Common Metals 26, 247 (1972).

34. Jung, W. D., Ph.D. Thesis (Iowa State University, 1975) (unpublished).

35. Bevington, P. R., Data Reduction and Error Analysis for the Physical Sciences, (McGraw-Hill, New York, 1969).

36. Petroff, I. and Viswanathan, C. R., Phys. Rev. B 4, 799 (1971).

37. Newrock, R. S. and Maxfield, B. W., Phys. Rev. B 7, 1283 (1972).

38. Bass, J., Adv. Phys. 21, 431 (1972).

ACKNOWLEDGMENTS

It is with great pleasure that I thank the following people for their varied skills in assisting me throughout this research. I extend my gratitude to my major professor, Dr. G. C. Danielson, for his continued encouragement and guidance. I also thank A. L. Bevolo for his assistance in data analysis. F. A. Schmidt provided the pure samples and was very helpful in characterizing them. I also thank O. M. Sevde for his invaluable technical assistance. I cannot fully express my gratitude to my parents, Jack and Maurine, for the encouragement and support only they could provide.